Effects of Metal-Centered Reduction on the Structural, Electronic, and Coordination Properties of Nickel and Copper Octaethylisobacteriochlorins

Mark W. Renner,*,† Lars R. Furenlid,*,‡ and Alan M. Stolzenberg§

Contribution from the Department of Applied Science and National Synchrotron Light Source, Brookhaven National Laboratory, Upton, New York 11973-5000, and Department of Chemistry, West Virginia University, P.O. Box 6045, Morgantown, West Virginia 26506-6045

Received June 27, 1994⊗

Abstract: The structural properties of nickel and copper complexes of octaethylisobacteriochlorin (OEiBC) are investigated as part of an effort to understand the chemistry of factor 430 (F430), the nickel hydrocorphinoid cofactor of methyl coenzyme-M reductase. Both Ni^{II} and Cu^{II}(OEiBC) undergo one-electron reductions to yield metal(I) complexes. The nature of the starting materials, the anionic metal(I) reduction products, and their ligand-binding properties are probed with electron paramagnetic resonance (EPR) and X-ray absorption techniques. Comparison between the structures of the isoelectronic Ni^{I} and Cu^{II} complexes reveals that the marked distortions observed in the Ni^{I}−macrocycle core environment, which has two Ni−N distances of 1.91(2) Å and two Ni−N distances of 2.07(2) Å, are not apparent for Cu^{II}, which has four Cu−N distances of 2.00(2) Å. Thus, the distortion of the Ni^{I} environment does not result from an electronic configuration effect such as a Jahn−Teller distortion. X-ray absorption near-edge studies of OEiBC complexes at reduced temperatures demonstrate for the first time that Ni^{I} hydroporphyrins can bind a single axial ligand. Optical and EPR spectra are found to be insensitive to the axial binding for these cases. Chemical reduction of Cu^{II}(OEiBC), using sodium amalgam, affords a Cu^{I} complex that has unchanged Cu−N distances and two sodium ions coordinated on opposite sides of the OEiBC ring at Cu−Na distances of 2.89(4) Å. The sodium ions can be sequestered using the crown ether 18-crown-6. Direct comparison of Cu^{II} and the non-ion-paired Cu^{I} complexes, which have the same geometry and coordination environment, establishes that the average Cu−N distance increases 0.06 Å upon reduction. The structural differences between the Ni^{I} and Cu^{I} complexes may account for their different reactivities toward alkyl halides and oxygen.

Introduction

Metal hydroporphyrins appear as cofactors in a diverse range of biological processes, including photosynthesis[1,2] and methanogenesis.[3,4] Hence, their structural and chemical properties are the object of considerable interest. Metalloisobacteriochlorins have been recently used as models[5−14] for the active sites in factor 430 (F430) containing enzymes[15,16] and in nitrite and sulfite reductases.[17−19]

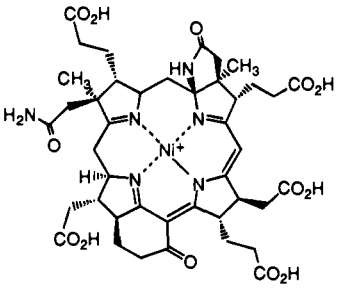

F430

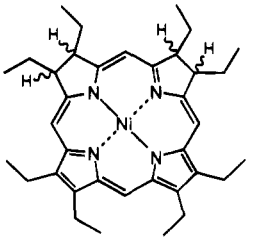

Ni(II)OEiBC

The nickel-hydrocorphinoid complex F430 is an essential cofactor in methyl-coenzyme M reductase (MCR), which catalyzes the final step in the reduction of CO_2 to methane in methanogenic bacteria.[20] The active form of F430 was proposed to be Ni^{I} from *in vitro* and *in vivo* electron paramagnetic resonance (EPR) studies.[21−25] Recent studies have established

† Department of Applied Science, Brookhaven National Laboratory.
‡ National Synchrotron Light Source, Brookhaven National Laboratory.
§ West Virginia University.
⊗ Abstract published in *Advance ACS Abstracts,* December 1, 1994.

(1) Feher, G.; Okamura, M. Y. In *Photosynthetic Bacteria*; Clayton, R. K., Sistrom, W. R., Eds.; Plenum Press: New York, 1978; p 349.
(2) Okamura, M. Y.; Feher, G.; Nelson, N. In *Photosynthesis*; Govingee, Ed.; Academic: New York, 1982; Vol. 1, p 195.
(3) Wolf, R. S. *Trends Biochem. Sci.* **1985**, *10*, 369.
(4) Ferry, J. G. *Crit. Rev. Biochem. Mol. Biol.* **1992**, *27*, 473.
(5) Fujita, E.; Fajer, J. *J. Am. Chem. Soc.* **1983**, *105*, 6743.
(6) Fujita, E.; Chang, C. K.; Fajer, J. *J. Am. Chem. Soc.* **1985**, *107*, 7665.
(7) Stolzenberg, A. M.; Strauss, S. H.; Holm, R. H. *J. Am. Chem. Soc.* **1981**, *103*, 4763.
(8) Stolzenberg, A. M.; Stershic, M. T. *Inorg. Chem.* **1987**, *26*, 1970.
(9) Stolzenberg, A. M.; Stershic, M. T. *Inorg. Chem.* **1988**, *27*, 1614.
(10) Stolzenberg, A. M.; Stershic, M. T. *J. Am. Chem. Soc.* **1988**, *110*, 6391.
(11) Stolzenberg, A. M.; Schussel, L. J. *Inorg. Chem.* **1991**, *30*, 3205.
(12) Stolzenberg, A. M.; Spreer, L. O.; Holm, R. H. *J. Am. Chem. Soc.* **1980**, *102*, 364.
(13) Furenlid, L. R.; Renner, M. W.; Smith, K. M.; Fajer, J. *J. Am. Chem. Soc.* **1990**, *112*, 1634.
(14) Renner, M. W.; Furenlid, L. R.; Barkigia, K. M.; Forman, A.; Shim, H.; Simpson, D. J.; Smith, K. M.; Fajer, J. *J. Am. Chem. Soc.* **1991**, *113*, 6891.
(15) Pfaltz, A.; Jaun, B.; Fassler, A.; Eschenmoser, A.; Jaenchen, R.; Gilles, H. H.; Deikert, G.; Thauer, R. K. *Helv. Chim. Acta* **1982**, *65*, 828.
(16) Ellefson, W. L.; Whitman, W. B.; Wolf, R. S. *Proc. Natl. Acad. Sci. U.S.A.* **1982**, *79*, 3707.
(17) Murphy, M. J.; Siegel, L. M.; Tover, S. R.; Kamin, H. *Proc. Natl. Acad. Sci. U.S.A.* **1974**, *71*, 612.
(18) Vega, J. M.; Kamin, H. *J. Biol. Chem.* **1977**, *252*, 896.
(19) Lancaster, J. R.; Vega, J. M.; Kamin, H.; Orme-Johnson, N. R.; Orme-Johnson, W. A.; Kreuger, R. H.; Siegel, L. M. *J. Biol. Chem.* **1979**, *254*, 1268.
(20) Rouviere, P. E.; Wolf, R. S. *J. Biol. Chem.* **1988**, *263*, 7913.
(21) Jaun, B.; Pfaltz, A. *J. Chem. Soc., Chem. Commun.* **1988**, 293.
(22) Jaun, B.; Pfaltz, A. *J. Chem. Soc., Chem. Commun.* **1986**, 1327.
(23) Albracht, S. P. J.; Ankel-Fuchs, D.; Van der Zwaan, J. W.; Fontjin, R. D.; Thauer, R. K. *Biochim. Biophys. Acta* **1986**, *870*, 50.
(24) Albracht, S. P. J.; Ankel-Fuchs, D.; Bocher, R.; Ellerman, J.; Moll, J.; Van der Zwaan, J. W.; Thauer, R. K. *Biochim. Biophys. Acta* **1988**, *955*, 86.

0002-7863/95/1517-0293$09.00/0

that reduction of low-spin Ni^{II} macrocycles to Ni^{I} requires both correctly ordered energies of the metal and macrocycle molecular orbitals and the ability of the macrocycle to accommodate the larger Ni^{I} ion.[10,13,26-28] In most cases studied to date, the Ni^{I}–macrocycle complex shows two distinct sets of Ni–N distances and a small expansion in the macrocycle core.[13,26-28] The origins of these structural features and their effects on the chemistry of the metal complex are unknown.

Measurements on whole cells of *Methanobacterium thermoautotrophicum* have revealed the presence of two EPR signals, MCR-red1 (axial) and MCR-red2 (rhombic), which were assigned to Ni^{I} forms of F430 in methyl-coenzyme M reductase.[23-25] Recent results demonstrate that the rhombic signal converts to the axial signal upon addition of substrates.[25] Hence, it has been proposed that the catalytic mechanism involves formation of an axial, nickel-to-sulfur bond between Ni^{I}(F430) and either the thioether substrate methyl-coenzyme M or the thiol cofactor H-S-HTP.[25,29] Isolated Ni^{I}(F430) exhibits a Ni^{I} EPR signal,[22,30] which is slightly rhombic, characteristic of a square-planar four-coordinate nickel. The different anisotropy between the native and isolated Ni^{I}(F430) might arise from presence of axial ligands in the former case. Clearly, knowledge of the ligand-binding properties of models for F430 will be important to an understanding of both the unusual and varied EPR signals and the reaction chemistry of the nickel cofactor.

One-electron reduction of both Ni^{II} and Cu^{II} octaethylisobacteriochlorins (OEiBC)[31] affords metal-centered rather than macrocycle π-system-centered reduction products.[8,10,11] Although formed at similar potentials, Ni^{I}(OEiBC)$^{-}$ shows greater rates of reaction toward alkyl halides and oxygen than Cu^{I}(OEiBC)$^{-}$. Unlike other Cu^{I} complexes, which form square-pyramidal complexes in the presence of added ligands, Cu^{I}(OEiBC)$^{-}$ has to date shown no evidence of coordination chemistry.[11] Recent resonance Raman (RR) studies of Ni^{II}-, Ni^{I}-, Cu^{II}-, and Cu^{I}(OEiBC) complexes indicated that reduction of the metal causes structural changes in the macrocycle.[32] Compared to low-spin Ni^{II}(OEiBC), larger frequency shifts were observed for high-spin Ni^{II}(OEiBC) than for Ni^{I}(OEiBC)$^{-}$. These results are consistent with previous extended X-ray absorption fine structure (EXAFS) and crystallographic studies of Ni^{I} macrocycles.[13,26-28] The RR data for Cu^{I}(OEiBC)$^{-}$ showed large shifts to lower frequencies for all macrocycle skeletal modes relative to Cu^{II}(OEiBC).

We present here the results of an investigation of the structural and ligand-binding properties of the Cu^{II}-, Cu^{I}-, Ni^{II}-, and Ni^{I}-(OEiBC) complexes. EXAFS and EPR measurements of the complexes in solution, both in the absence and presence of added ligands, are used to determine the coordination number, the coordination geometry, and the metal–ligand distances. Comparison of the structural features of the isoelectronic Cu^{II}- and Ni^{I}(OEiBC) complexes permits us to determine whether the two distinct sets of metal–nitrogen distances observed for other Ni^{I} complexes is a general feature of d^9 complexes and thus arises from the electronic configuration. Comparison of the Cu^{II}- and Cu^{I}(OEiBC) complexes provides an opportunity both to examine the effect of reduction on the Cu–ligand bond lengths when the coordination environment is conserved and to explain the RR observations for Cu^{I}(OEiBC)$^{-}$.

Experimental Section

Tetrahydrofuran (THF) was dried by distillation from sodium–benzophenone, and pyridine was dried by distillation from 4 Å molecular sieves prior to use. The 18-crown-6 ether was purified by recrystallization from hot acetonitrile and dried under vacuum.[33] Synthesis of Ni^{II}- and Cu^{II}(OEiBC) was described previously.[10,12]

All samples were prepared as ~2 mM THF solutions using vacuum techniques in EXAFS cells of published design.[34] The ligand-binding studies were carried out with an excess of pyridine present. The Cu^{II} and Ni^{II} were reduced using 0.1% sodium–amalgam and monitored with optical absorption spectroscopy. The five-coordinate Ni^{I}(OEiBC)$^{-}$–pyridine complex was generated by reduction of the Ni^{II} sample followed by distillation of an excess of pyridine into the cell. Initial EXAFS experiments indicated that a sodium cation might be coordinated to the Cu^{I}. Therefore, we repeated the experiment in the presence of 18-crown-6 ether.

Optical spectra were recorded on a Hewlett-Packard 8452A diode array spectrophotometer. EPR spectra were measured on a Bruker-IBM ER200 spectrometer equipped with an Aspect 2000 data acquisition system. The Ni^{I} EPR spectra were simulated with a program kindly provided by T. D. Smith and P. Aisen of the Albert Einstein College of Medicine.[35]

X-ray absorption experiments were performed at the National Synchrotron Light Source on beamlines X-9B, X-10C, X-11A, and X-19A. Data were collected with Si 111 (X-9B), Si 220 (X-10C), Si 311 (X-11A), and Si 220 (X-19A) monochromator crystals with slits adjusted to give ~1–2 eV resolutions. The samples were measured in fluorescence mode with either a Canberra 13-element solid state detector or a Lytle ionization detector. Enough 20-min energy scans were collected to yield an edge step of $>10^6$ counts of fluorescence photons. Dead time effects in the solid state detector were minimized by restricting total count rates to less than 25 000 counts/s with a 0.5 μs shaping time. The absolute energy positions were calibrated with a Ni (8333 eV) or Cu (8979 eV) metal foil, and no changes in energy scale were observed over the course of the experiments. Data for Ni^{II}-(OEP) and Cu^{II}(TPP) were collected under the same conditions for use as calibration standards. Samples were cooled using a liquid nitrogen cryostat (CRYO Industries of America, Inc.).

Sample purities were monitored before and after X-ray exposure. The integrity of the Cu^{II} and Ni^{II} samples were unchanged upon exposure to X-rays. However, the Cu^{I} without crown ether and Ni^{I} samples in THF decomposed back to the starting materials with prolonged X-ray exposure at room temperature. This decay could be monitored by observing changes in the X-ray absorption near-edge structure (XANES) spectra. Experiments run at 150 K or lower showed no change in the XANES region throughout the data collection; however, upon warming to room temperature, Cu^{I} and Ni^{I} were reoxidized. This suggests that the metal(I) species only decompose upon warming. In the experiment run in the presence of 18-crown-6 at 110 K, no Cu^{I} decomposition, as monitored by XANES and optical spectra, was noted upon warming to room temperature.

The data were analyzed with the MacXAFS EXAFS analysis package.[36] The EXAFS oscillations for the samples and standards were

(25) Rospert, S.; Voges, M.; Berkessel, A.; Albracht, S. P. J.; Thauer, R. K. *Eur. J. Biochem.* **1992**, *210*, 101.

(26) Suh, M. P.; Kim, H. K.; Kim, M. J.; Oh, K. Y. *Inorg. Chem.* **1992**, *31*, 3620.

(27) Furenlid, L. R.; Renner, M. W.; Fajer, J. *J. Am. Chem. Soc.* **1990**, *112*, 8987.

(28) Furenlid, L. R.; Renner, M. W.; Szalda, D. J.; Fujita, E. *J. Am. Chem. Soc.* **1991**, *113*, 883.

(29) Berkessel, A. *Bioorg. Chem.* **1991**, *19*, 101.

(30) Hollinger, C.; Pierik, A. J.; Reijerse, E. J.; Hagen, W. R. *J. Am. Chem. Soc.* **1993**, *115*, 5651.

(31) Abbreviations: OEP, 2,3,7,8,12,13,17,18-octaethylporphyrin dianion; OEiBC, mixture of *ttt*- and *tct*-2,3,7,8-tetrahydro-2,3,7,8,12,13,17,18-octaethylporphyrin dianion (isobacteriochlorin); TPP, 5,10,15,20-tetraphenylporphyrin dianion; dioxoOEiBC, 3,8-dioxo-2,2′,7,7′,12,13,17,18-octaethylporphyrin diamion; H-S-HTP, 7-mercaptoheptanoylthreonine phosphate; F430M, coenzyme F430 pentamethyl ester; NMR, nuclear magnetic resonance.

(32) Procyk, A. D.; Stolzenberg, A. M.; Bocian, D. F. *Inorg. Chem.* **1993**, *32*, 627.

(33) Gokel, G. W.; Cram, D. J.; Liotta, C. L.; Harris, H. P.; Cook, F. L. *J. Org. Chem.* **1974**, *39*, 2445.

(34) Furenlid, L. R.; Renner, M. W.; Fajer, J. *Rev. Sci. Instrum.* **1990**, *61*, 1326.

(35) Toy, A. D.; Chaston, S. H. H.; Smith, T. D. *Inorg. Chem.* **1971**, *10*, 2219.

(36) Bouldin, C. E.; Elam, W. T.; Furenlid, L. R. *Physica B*, in press.

isolated with standard methods:[37,38] linear extrapolation and subtraction of a pre-edge bulk-absorption contribution, normalization of the edge step, interpolation onto a photoelectron momentum (k) grid, and removal of a smooth background with a series of three cubic splines. E_0 was defined as the energy corresponding to the midpoint of the main absorption step. The resulting oscillations were weighted with k^3 factors and Fourier-filtered to isolate first-shell contributions as amplitude and phase functions. Quantitative comparisons between the unknown and standards were accomplished with nonlinear fits based on the generalized EXAFS equation:

$$\chi(k) = \sum_i \frac{N_i}{kr_i^2} f_i(k,r_i) e^{-2k^2\sigma_i^2} \sin(2kr_i + \theta_i(k,r_i))$$

and verified with theoretical simulations carried out with FEFF 3.11,[39,40] an *ab initio*, curved-wave, single-scattering EXAFS simulation code.

Results

X-ray Absorption Spectroscopy. Near-Edge Spectra. The X-ray absorption near-edge structure (XANES) for organometallic complexes contains both structural and chemical information. In transition metal complexes that contain empty 3d orbitals, a symmetry forbidden 1s−3d transition ("pip") about 10 eV below the metal absorption edge is observed.[41,42] The intensity of this peak can be sensitive to structural and coordination changes around the metal; in noncentrosymmetric geometries, the transition gains dipole character due to 3d−4p orbital mixing.[43,44] Hence, the "pip" is weak for square-planar but is enhanced in five- and distorted four- and six-coordinate complexes of cobalt, for example.[45] However, in square-planar Ni^{II} the unoccupied $d_{x^2-y^2}$ orbital is oriented in the xy plane, and does not gain p character from loss of inversion symmetry in the z direction.

About 6 eV below the absorption edge, a peak assigned to a $1s \rightarrow 4p_z$ transition has also been shown to be sensitive to the geometry and coordination of the metal. In the case of square-planar Ni^{II} (d^8) and Ni^{I} (d^9) complexes,[13,14,28,46,47] the $1s \rightarrow 4p_z$ peak intensity is inversely correlated with the number of axial ligands in the metal's coordination environment, thereby providing a convenient marker for studies of ligand binding to Ni. The effect can be interpreted to result from the ligands' charge density raising the $4p_z$ orbital energy. However, a similar pre-edge peak observed with Cu^{II} complexes appears less sensitive to the absence or presence of axial ligands. A possible explanation is that since the Jahn−Teller distortion present in octahedral (d^9) systems generally results in much longer axial bond lengths, the overlap of charge density is less. To date, theoretical efforts to fully explain the Cu pre-edge features concur that the peak is a $4p_z$ type transition but have reached a variety of conclusions about the importance of higher order processes such as shake down.[48−50] The attenuation of $4p_z$ peak intensity could also formally result from a change toward a tetrahedral coordination environment; however, no such symmetries have been observed or are likely in metalloporphyrins.

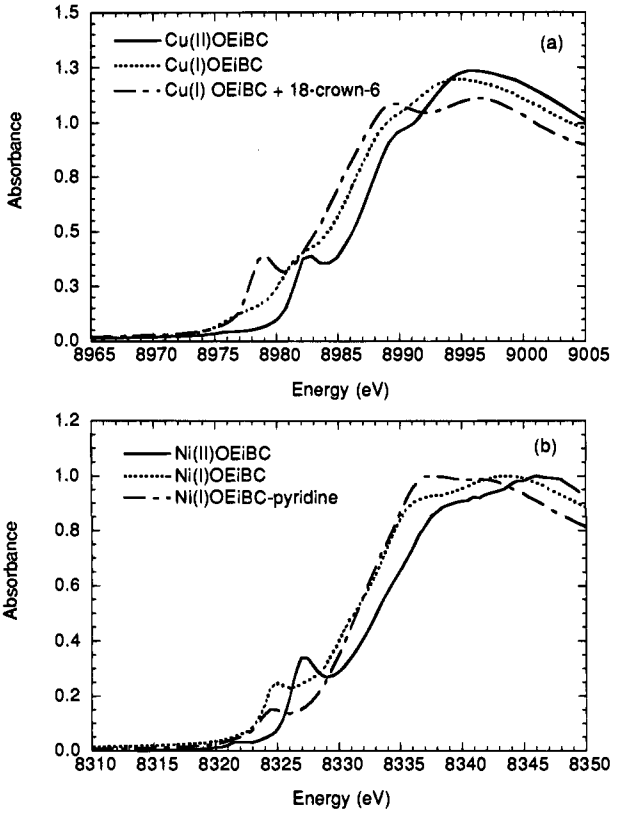

Figure 1. X-ray absorption near-edge spectra for (a) Cu^{II}(OEiBC), Cu^{I}(OEiBC)$^-$, and Cu^{I}(OEiBC)$^-$ plus crown ether, all in THF at 300, 150, and 110 K, respectively, and (b) Ni^{II}(OEiBC), Ni^{I}(OEiBC)$^-$, and Ni^{I}(OEiBC)$^-$-(pyridine) in THF at 300, 110, and 130 K, respectively.

The overall edge energy position is sensitive to the metal's oxidation state, provided that the molecular geometry is roughly constant. For transition metals, a 2−3 eV change in the edge energy is observed per one electron reduction or oxidation, with edges shifting to lower energies in the former case, higher in the latter.[13,27,28] These trends have been confirmed for a number of model systems, including Cu and Ni complexes.

Comparison of the XANES spectra for the Cu^{II}(OEiBC) and Cu^{I}(OEiBC)$^-$, Figure 1a, and Ni^{II}(OEiBC) and Ni^{I}(OEiBC)$^-$, Figure 1b, shows the characteristic decrease in the edge energy consistent with metal-centered reductions. When Cu^{II}(OEiBC) was reduced without the addition of crown ether, the edge shifts approximately −2 eV relative to Cu^{II} and shows a less-resolved $4p_z$ pre-edge feature. Also evident is an enhancement in the quadrupole allowed 1s−3d "pip",[51] suggesting a different coordination geometry. For Cu(OEiBC) with crown ether and Ni(OEiBC), the reduction products show main absorption edge shifts of −3 eV and $4p_z$ pre-edge peaks with comparable

(37) Teo, B. K. In *EXAFS: Basic Principles and Data Analysis*; Springer-Verlag: Berlin, 1986.
(38) Stern, E. A.; Heald, S. M. In *Handbook on Synchrotron Radiation*; Koch, E. E., Ed.; Springer-Verlag: North Holland, Amsterdam, 1983.
(39) Rehr, J. J.; Balci, M.; Pramod, K.; Koch, P.; Lex, J.; Ermer, O. *J. Am. Chem. Soc.* **1991**, *113*, 5135.
(40) Mustre de Leon, J.; Rehr, J. J.; Zabinsky, S. I. *Phys. Rev. B* **1991**, *44*, 4146.
(41) Hu, V. W.; Chan, S. I.; Brown, G. S. *Proc. Natl. Acad. Sci. U.S.A.* **1977**, *74*, 3821.
(42) Shulman, R. G.; Yafet, Y.; Eisenberg, P.; Blumberg, W. E. *Proc. Natl. Acad. Sci. U.S.A.* **1976**, *73*, 1384.
(43) Roe, A. L.; Schneider, D. J.; Mayer, R. J.; Pyrz, J. W.; Widom, J.; Que, L., Jr. *J. Am. Chem. Soc.* **1984**, *106*, 1676.
(44) Wong, J.; Lytle, F. W.; Messmer, R. P.; Maylotte, D. H. *Phys. Rev. B* **1984**, *30*, 5596.
(45) Wirt, M. D.; Sagi, I.; Chen, E.; Frisbie, S. M.; Lee, R.; Chance, M. R. *J. Am. Chem. Soc.* **1991**, *113*, 5299.
(46) Eidsness, M. K.; Sullivan, R. J.; Schwartz, J. R.; Hartzell, P. L.; Wolfe, R. S.; Flank, A.; Cramer, S. P.; Scott, R. A. *J. Am. Chem. Soc.* **1986**, *108*, 3120.
(47) Schiemke, A. K.; Kaplan, W. A.; Hamilton, C. L.; Shelnutt, J. A.; Scott, R. A. *J. Biol. Chem.* **1989**, *264*, 7276.
(48) Kosugi, N.; Yokoyama, T.; Asakura, K.; Kuroda, H. *Chem. Phys.* **1984**, *91*, 249.
(49) Doniach, S.; Berding, M.; Smith, T.; Hodgson, K. O. In *EXAFS and Near Edge Structure III*; Hodgson, K. O., Hedman, B., Penner-Hahn, J. E., Eds.; Springer: New York, 1983; p 33.
(50) Bair, R. A.; Goddard, W. A., III. *Phys. Rev. B* **1980**, *22*, 2767.
(51) Bunker, G.; Stern, E. A.; Blankenship, R. E.; Person, W. *Biophys. J.* **1982**, *37*, 539.

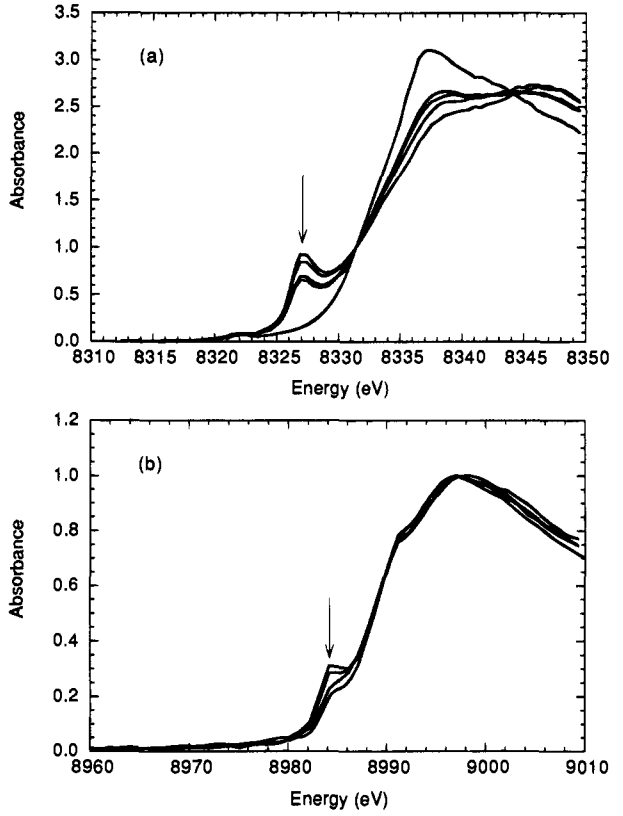

Figure 2. Temperature dependence of the X-ray absorption near-edge spectra for (a) Ni^{II}(OEiBC) in THF/pyridine (T = 300−130 K) and (b) Cu^{II}(OEiBC) in THF/pyridine (T = 300−150 K). The arrows indicate the directions of change as the temperature decreases.

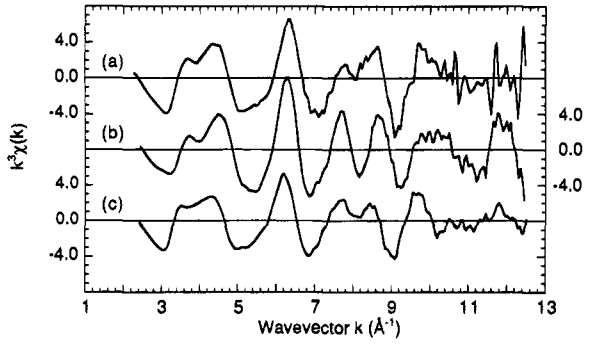

Figure 3. Isolated k^3-weighted EXAFS oscillations for (a) Cu^{II}(OEiBC) at 300 K, (b) Cu^{I}(OEiBC)$^-$ at 150 K, and (c) Cu^{I}(OEiBC)$^-$ with crown ether at 110 K. All samples in THF.

intensity. This indicates that in both cases the metal remains four-coordinate and square-planar.

Edge spectra from temperature dependent ligand-binding studies of Ni^{II}-, Ni^{I}-, and Cu^{II}(OEiBC) with pyridine are shown in Figures 1b and 2. At room temperature, all species remain four-coordinate. Upon cooling, Ni^{II}(OEiBC) can be seen to cleanly convert to a high-spin six-coordinate species from the full attenuation of the $4p_z$ peak, whereas for Ni^{I}- and Cu^{II}-(OEiBC), the partial attenuation indicates the binding of only a single axial ligand. Experiments showed no evidence for the binding of CO to Ni^{I} at any temperature.

EXAFS. The isolated and k^3-weighted EXAFS oscillations for the Ni- and Cu(OEiBC) complexes are shown in Figures 3 and 4. Fourier transforms calculated over a k range of approximately 3−12 Å^{-1} are presented in Figures 5 and 6. Visual inspection of the raw and transformed data reveals a significant difference between Ni^{II} and Ni^{I}, the latter displaying

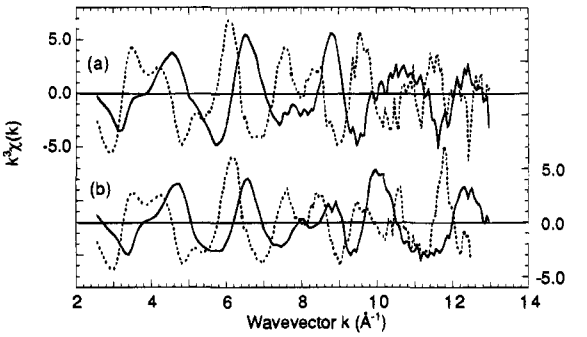

Figure 4. Isolated k^3-weighted EXAFS oscillations for (a) Ni^{II}(OEiBC) (—) at 300 K and Ni^{II}(OEiBC)(pyridine)$_2$ (- - -) at 130 K and (b) Ni^{I}(OEiBC)$^-$ (—) at 110 K and Ni^{I}(OEiBC)$^-$(pyridine) (- - -) at 130 K. All samples in THF.

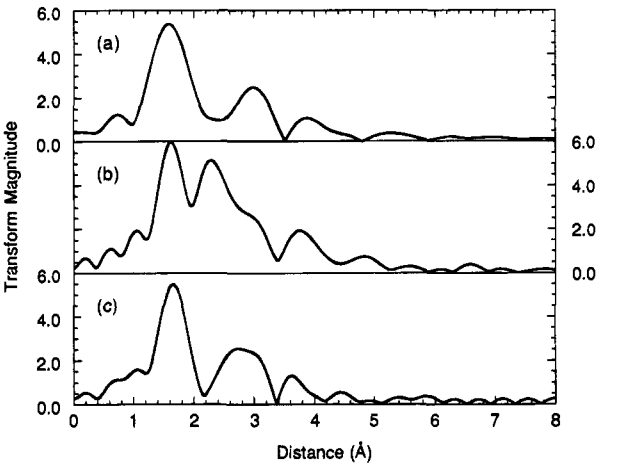

Figure 5. Fourier transform magnitudes of the k^3-weighted EXAFS oscillations of (a) Cu^{II}(OEiBC), (b) Cu^{I}(OEiBC)$^-$, and (c) Cu^{I}(OEiBC)$^-$ with crown ether.

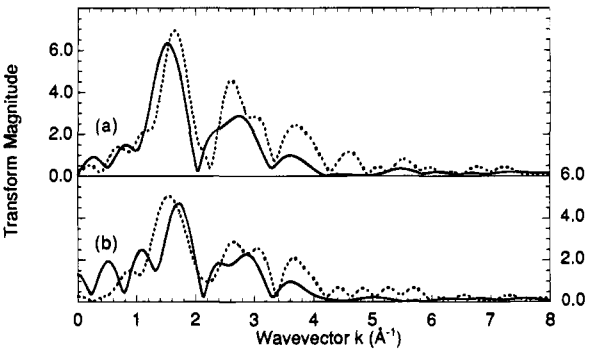

Figure 6. Fourier transform magnitudes of the k^3-weighted EXAFS oscillations of (a) Ni^{II}(OEiBC) (—) and Ni^{II}(OEiBC)(pyridine)$_2$ (- - -) and (b) Ni^{I}(OEiBC)$^-$ (—) and Ni^{I}(OEiBC)$^-$(pyridine) (- - -).

evidence for a beat in the amplitude at k ~8−9 Å^{-1} and attenuation of the first-shell peak in the transform consistent with increased disorder as observed in other Ni^{I} hydroporphyrins. Only smaller effects are observed for Cu^{II} to Cu^{I} reduction, with an evident small phase shift in the raw data, which results in a first-shell distance shift in the transform.

The transform of Cu^{I}(OEiBC)$^-$ generated in the absence of 18-crown-6 shows an unexpectedly large second shell. An analysis of the k-weighting dependent intensity of this peak, which amplifies the k dependence of atomic backscattering amplitudes, suggests that it is the result of a higher z element present in the first coordination sphere, see Figure 7. This peak

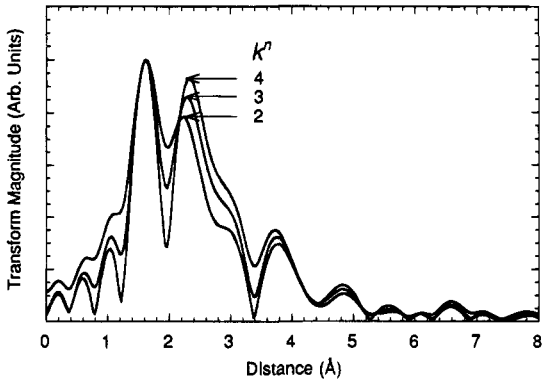

Figure 7. Fourier transform magnitudes of k^n EXAFS oscillations of $Cu^{I}(OEiBC)^-$ (without crown ether), $n = 2, 3, 4$. Transforms were normalized to the intensity of the first-shell peak.

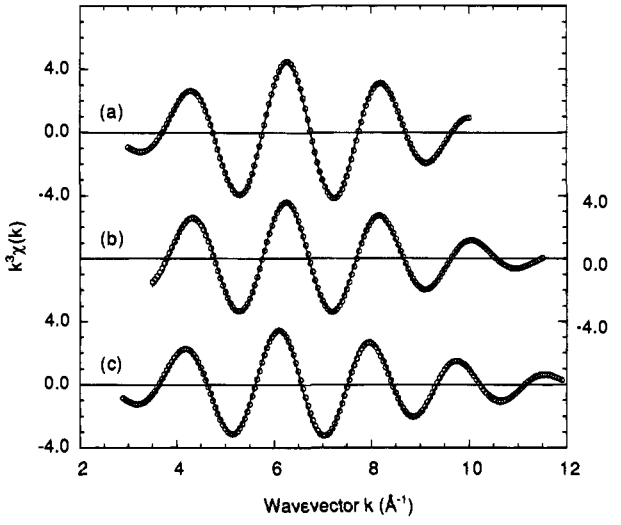

Figure 8. Fourier-filtered first-shell EXAFS oscillations (—) and nonlinear least-squares fits (O) of (a) $Cu^{II}(OEiBC)$, 4 N at 2.00 Å; (b) $Cu^{I}(OEiBC)^-$, 4 N at 2.01 Å; and (c) $Cu^{I}(OEiBC)^-$ with crown ether, 4 N at 2.06 Å.

is not present when experiments are carried out in the presence of crown ether added to sequester sodium ions.

The addition of pyridine ligands to Ni^{I}- and $Ni^{II}(OEiBC)$ also results in visible changes to the isolated EXAFS oscillations and transforms. In both cases, there is an evident shift of the first shell to larger average distances and a decrease in the transform amplitude consistent with increased disorder. The isolated first-shell Ni^{I} EXAFS also shows the attenuation in the amplitude associated with a distribution of significantly different distances.

Filtered first-shell EXAFS oscillations and associated nonlinear, least-squares fits are shown in Figures 8 and 9 and presented quantiatively in Table 1. $Ni^{II}(OEiBC)$ was quantitatively compared to a single scattering standard simulated with the FEFF 3.11 EXAFS code.[39,40] The isolated first shell is adequately fit with nitrogens at a single average distance of 1.94 Å. The low coordination number of 2.8 is the result of neglect of many-body interactions in the theory and is consistent with calibrations against known standards such as Ni(OEP). The edge spectrum also independently verifies the four-coordinate nature of the sample. The $Ni^{II}(OEiBC)$ was then used as the experimental standard for comparison against the remaining Ni samples.

$Ni^{I}(OEiBC)^-$ at 110 K also appears to be four-coordinate from its edge and quantitative EXAFS analysis, but fits with only a single average distance yield unacceptably large good-

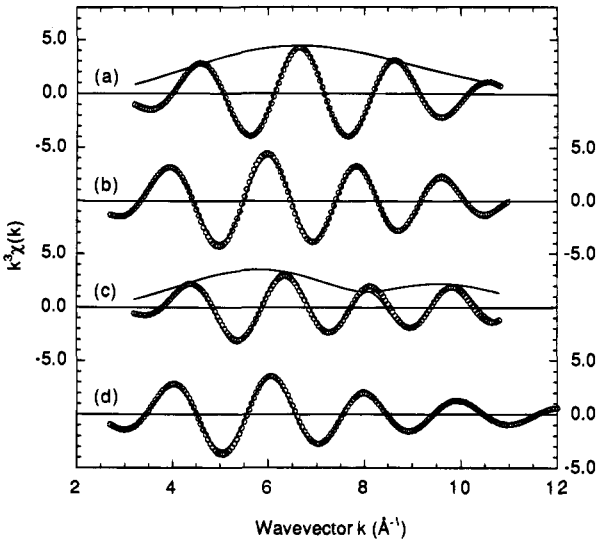

Figure 9. Fourier-filtered first-shell EXAFS oscillations (—) and nonlinear least-squares fits (O) for (a) $Ni^{II}(OEiBC)$, 4 N at 1.94 Å; (b) $Ni^{II}(OEiBC)(pyridine)_2$, 2 N at 2.08 Å and 4 N at 2.09 Å; (c) $Ni^{I}(OEiBC)^-$, 2 N at 2.07 and 1.91 Å; and (d) $Ni^{I}(OEiBC)^-$(pyridine), 2 N at 2.0 Å and 3 N at 2.13 Å. The amplitude functions are included in traces (a) and (c) to better illustrate the beating in the latter case.

Table 1. Nickel and Copper Octaethylisobacteriochlorin EXAFS Results[a]

compound	temp (K)	N	R (Å)	$\Delta\sigma^2$ (Å^2)	χ^2 (gof)	ΔE_0 (eV)
$Ni^{II}(OEiBC)$[b]	300	2.8	1.94	0.002	0.014	−3
$Ni^{II}(OEiBC)(pyr)_2$[c,d]	130	5.2	2.09	0.0011	0.012	3
$Ni^{II}(OEiBC)(pyr)_2$[c,d]	130	6.0[e]	2.09	0.003	0.036	3
$Ni^{I}(OEiBC)^-$ [c,d]	110	4.2	2.04	0.004	0.375	−3
$Ni^{I}(OEiBC)^-$ [c]	110	3.0[e]	1.96	0.004	0.100	0
		1.0[e]	2.08	−0.008		
$Ni^{I}(OEiBC)^-$ [c]	110	2.0[e]	1.91	0.000	0.090	0
		2.0[e]	2.07	−0.006		
$Ni^{I}(OEiBC)(pyr)^-$ [c,d]	130	6.3	2.07	0.007	0.078	3
$Ni^{I}(OEiBC)(pyr)^-$ [c]	130	5.0[e]	2.06	0.004	0.118	3
$Ni^{I}(OEiBC)(pyr)^0$ [c]	130	4.0[e]	2.04	−0.001	0.023	3
		1.0[e]	2.20	−0.004		
$Ni^{I}(OEiBC)(pyr)^-$ [c]	130	2.0[e]	2.00	−0.002	0.026	3
		3.0[e]	2.13	0.000		
$Cu^{II}(OEiBC)$[f]	300	4.2	2.00	0.001	0.004	−1
$Cu^{I}(OEiBC)^-$ [g]	150	4.5	2.01	0.003	0.007	−3
$Cu^{I}(OEiBC)^-$ [h]	110	3.8	2.06	0.002	0.012	−3
$Cu^{I}(OEiBC)^-$ [g,i]	110	2.0[e]	2.89	−0.003	0.055	10
		8.0[e]	3.09	0.004		
		4.0[e]	3.34	−0.005		

[a] N is the coordination number per metal. The metal-coordinating atom distance (R) is determined from fits of the first-shell EXAFS data. $\Delta\sigma^2$ is the relative mean square deviation in R (the square of the Debye–Waller factor), $\Delta\sigma^2 = \sigma^2_{unknown} - \sigma^2_{std}$. χ^2_{gof} is a relative goodness-of-fit statistic, defined as $\Sigma(exp-fit)^2/\Sigma exp^2$. Experimental details: k range ~3.3–10.5, Hanning window = 0.5 Å^{-1}, weighting k^3, R window ~0.8–2.2 Å, Hanning window ~0.1 Å. [b] FEFF standard 4 N at 1.95 Å. [c] $Ni^{II}(OEiBC)$ standard. [d] Single shell fit. [e] Fixed N. [f] $Cu^{II}TPP$ standard (Cu–N distances of 2.00 Å). [g] 0.1% Na/Hg reduction in THF without 18-crown-6, first-shell fit using $Cu^{II}(OEiBC)$ as the standard. [h] 0.1% Na/Hg reduction in THF in the presence of 18-crown-6, first-shell fit using $Cu^{II}(OEiBC)$ as the standard. [i] Isolated second-shell EXAFS oscillations fit using FEFF-generated Cu–Na and Cu–C standards.

ness-of-fit (gof) indices. Therefore, the first shell is modeled as consisting of two independent distances. In order to keep the number of free parameters consistent with the experimentally accessible k and r ranges, the coordination numbers (N) were not varied; they were instead fixed at $N_1/N_2 = 2/2$ and $N_1/N_2 = 3/1$. In the best fit, the gof is improved by a factor of ~4, and there are two sets of two nitrogens with distances of 1.91 and

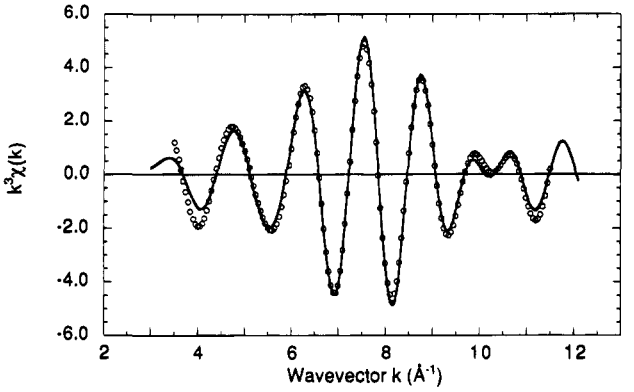

Figure 10. Goodness-of-fit indices for fits with two shells at fixed distance differences for Ni^{II}(OEiBC) (◇) and Ni^{I}(OEiBC)$^-$ (○). Fits were carried out with $N_2 = N_1$ and $R_2 = R_1 + \Delta R$. Free parameters were N_1, R_1, σ_1^2, and σ_2^2.

2.07 Å. This 0.16 Å distortion is consistent with the presence of the amplitude beat, see Figure 9c, which would predict two distances differing by roughly 0.2 Å.[38]

In order to strengthen the evidence for the presence of two distinct equatorial distances in the Ni^{I}(OEiBC)$^-$ sample, a series of two-shell fits were performed for both Ni^{II} and Ni^{I} in which the separation between the two distances was varied in fixed increments from 0 (a single shell) to 0.26 Å. The resulting correlations between the gof index and ΔR are presented in Figure 10. The gof index for the Ni^{II} sample, which has only a single shell, is largely independent of the addition of a second shell at any distance separation. Analysis of the fitting parameters reveals that the EXAFS contributions from the added second shell are negated via a large Debye–Waller factor. However, for the Ni^{I} sample, a very different behavior is observed, with a well-defined minimum in the gof index at a distance separation of 0.16 Å. This supports the observation of a significant structural change upon reduction of Ni^{II}(OEiBC).

Ni^{II}(OEiBC) in the presence of pyridine at 130 K gives a single-shell fit of 5.2 nitrogens at 2.09 Å, with a gof of 0.012. Fixing N at 6, consistent with the XANES results, leaves the distance unchanged, but results in a small increase in the gof to 0.036. Attempts at fitting with two shells, to account for the presumably longer axial bonds, were unsuccessful in resolving a second distance. Ni^{I}(OEiBC)$^-$ with pyridine at 130 K, which appears five-coordinate from the XANES, shows a single-shell result of six nitrogens at 2.07 Å. Restricting the coordination number to 5 gave a worse gof. Splitting the first shell into two distinct distances with $N_1/N_2 = 4/1$ or 3/2 once again resulted in better agreement with experiment and reasonable models for ligation by a single axial pyridine. Both fits have comparable gof indices, but the model with two nitrogens at 2.0 Å and three nitrogens at 2.13 Å has more physically reasonable Debye–Waller factors than the model with four nitrogens at 2.04 Å and one nitrogen at 2.2 Å.

The isolated first-shell fits for both Cu^{II}(OEiBC) and Cu^{I}(OEiBC)$^-$ without crown ether yield Cu–N distances of 2.00 Å. The Cu^{I} sample generated in the presence of the crown ether has an average Cu–N distance of 2.06 Å. All samples fit adequately and give reasonable Debye–Waller factors with a simple model of four nitrogens at a single distance, see Table 1 and Figure 8. A quantitative analysis of the second shell for Cu^{I}(OEiBC)$^-$ in the absence of crown ether is also presented in Table 1. Comparison of the transform with that of Cu^{II} reveals that the second-shell peak contains contributions from multiple atoms. Analysis of porphyrin structures reveals that two carbon types fall within the distance range isolatable with

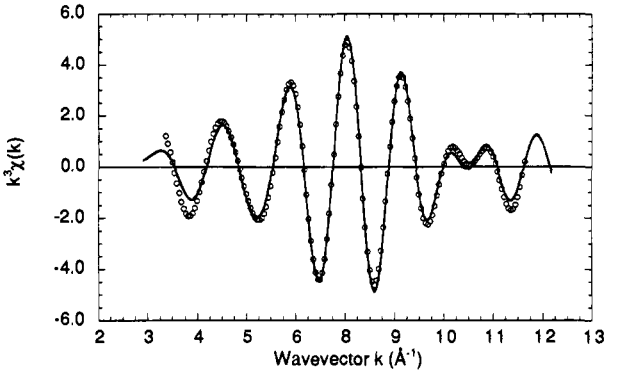

Figure 11. Fourier-filtered second-shell EXAFS oscillations (—) and nonlinear least squares fits (○) of Cu^{I}(OEiBC)$^-$ without crown ether 2 Na at 2.89 Å, 8 C at 3.09 Å, and 4 C at 3.34 Å.

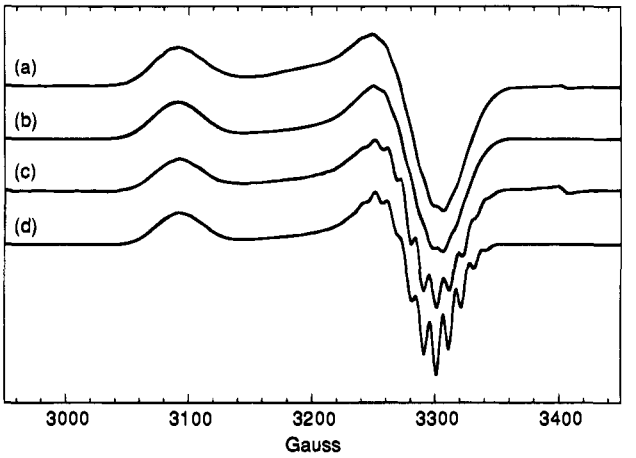

Figure 12. The EPR spectra and simulations for Ni^{I}(OEiBC)$^-$ ((a) and (b)) and Ni^{I}(OEiBC)$^-$ plus pyridine ((c) and (d)) in THF at 113 K. The $g_{x,y,z}$, A_N, and line $width_{x,y,z}$ used in the simulations: (b) $g = 2.061$, 2.083, 2.2025; $A_N = 9.8$ G; line $width_{x,y,z} = 9.5$, 9.5, 20 G and (d) $g =$ 2.065, 2.082, 2.2035; $A_N = 10.3$ G; line $width_{x,y,z} = 6.0$, 6.0, 6.0 G.

Fourier filtering. Thus second-shell FEFF models, which include the α- and meso-carbons of the OEiBC skeleton and one or two heavier atoms, were constructed. Best nonlinear-squares fits were found to require two sodium atoms at 2.89 Å, eight carbons at 3.09 Å, and four carbons at 3.34 Å. The simulated EXAFS data agree well with the complicated pattern of second-shell oscillations observed experimentally, see Figure 11.

Optical and EPR Spectroscopy

The optical absorption spectra of the starting materials and reduction products agree with previously published results.[8,11] Presence of crown ether during the reduction of Cu^{II} to Cu^{I} did not affect the optical properties. It should be noted that the optical spectra of the Cu^{II}- and Cu^{I}(OEiBC) complexes are not markedly different. EPR spectra for Ni^{I}(OEiBC)$^-$ are shown in Figure 12a together with a simulation with the specified parameters. The g values and nitrogen coupling constant are consistent with a single electron localized in the Ni $d_{x^2-y^2}$ orbital in a square-planar environment. Addition of pyridine as a coordinating base results in only a subtle change in the EPR spectrum, increased resolution in the $g_\perp$ signal. The g values and nitrogen coupling constant are otherwise similar, see Figure 12. Adequate simulations were obtained using only the four nitrogens of the macrocyle core.

Discussion

Recent studies on isolated F430 and related Ni hydroporphyrins have demonstrated that reduction to Ni^{I} results in significant changes in the metal−macrocycle structure.[13,27,28,32] For all cases studied to date, a significant distortion away from a symmetric square-planar arrangement is observed. It has not been clear whether this reflects an inherent property of Ni^{I} or is an exaggeration of the different types of bonds the metal can form with the chemically different nitrogens present in the macrocycle core. The highly saturated F430 macrocycle is extremely flexible and readily accommodates nickel in a variety of oxidation states: Ni^{I}, high- and low-spin Ni^{II}, and Ni^{III}.[21,47,52-54] Systematic crystallographic studies have revealed that short metal−nitrogen distances are associated with highly ruffled macrocycle structures.[55]

The metallooctaethylisobacteriochlorins studied here exist as a mixture of two stereoisomers, the *ttt* and *tct* relative orientations of the ethyl groups on the saturated rings. Crystal structures for the *ttt*- and *tct*-isomers reveal similar macrocycle ruffling and average Ni−N distances of 1.918 and 1.942 Å, respectively.[56] The electronic and vibrational properties for these two isomers are essentially identical in solution.[57] However, the *ttt* form has a greater ligand-binding constant (4−6 times greater) than the *tct* form,[57] but *tct* is the more thermodynamically stable isomer.[56]

The current EXAFS study established that in solution Ni^{II}(OEiBC) has an average metal−nitrogen bond length of 1.94 Å, similar to that found in crystal structures of Ni^{II}(OEiBC).[56] This slightly longer than the 1.90 Å average distance found in low-spin Ni^{II}(F430M).[27] The small Debye−Waller factor indicates that the two isomers of Ni^{II}(OEiBC) are structurally indistinguishable. The high-spin Ni^{II} complex that results from ligation of two axial pyridines was found to have average bond lengths of 2.09 Å, which is comparable to the average distance of 2.10 Å found in high-spin F430 in isolated and whole enzyme form.[46,47] However, in the F430 case and other investigated high-spin nickel porphyrins, the coordination geometry is split into shorter equatorial metal−nitrogen bonds (~2.00 Å) and considerably longer axial bonds (~2.2 Å). Difficulties in detecting such a split in high-spin Ni^{II}(OEiBC) could result from the presence of the two isomers, which might have slightly different bond lengths. The near-edge structure clearly indicates that the nickel is six-coordinate, and optically the two high-spin complexes are similar.[57]

The reduction of Ni^{II}(OEiBC) was also found to result in a Ni^{I} environment very similar to that in reduced F430M.[27] The Ni−N distances were split into two sets differing by 0.16 Å, with an average length increase of 0.05 Å compared to the low-spin Ni^{II}. Similar results have been observed in all EXAFS and crystallographic studies of Ni^{I} hydroporphyrins and tetraazamacrocycles to date.[13,26-28] The metal environment in Ni(OEiBC) thus appears consistently similar to that in F430. The OEiBC macrocycle is perhaps somewhat less flexible, as evidenced by the longer low-spin Ni^{II} distances, in agreement with fewer sites of saturation.

In these EXAFS studies of Ni(OEiBC), the metal−macrocycle core bond lengths vary as high-spin Ni^{II} > Ni^{I} (four- and five-coordinate) > low-spin Ni^{II}. This correlates with the occupancy of the metal $d_{x^2-y^2}$ orbital and the degree of coordinative saturation. The measured trend in the bond lengths is in agreement with the previously reported trend in RR skeletal mode frequencies.[32]

The discovery of binding by a single pyridine to Ni^{I}(OEiBC)$^-$ is the first observation of axial ligation in Ni^{I} hydroporphyrins.[58] Previous optical studies of Ni^{I}(OEiBC)$^-$ and isolated F430M have suggested that the Ni^{I} remains four-coordinate in the presence of a variety of bases.[53,59] However, the optical and EPR spectra were found here to be insensitive to the presence of axial ligands. The increased resolution in the $g_\perp$ EPR signal of Ni^{I} noted upon coordination by an axial ligand has been previously observed for the binding of sulfur dioxide to Ni^{I} thiaporphyrin.[60,61] The origin of this effect is still not clear.

The X-ray absorption $4p_z$ near-edge feature, which directly probes the presence of axial ligands, provided unambiguous confirmation that the Ni^{I} was five-coordinate at cold temperatures. The inability to detect hyperfine coupling due to the axial nitrogen in the EPR spectra implies that there is little overlap between the Ni $d_{x^2-y^2}$ orbital and the axial pyridine. A similar effect has been observed in EPR and ENDOR studies of isoelectronic Cu^{II} systems,[6,62] and electron spin echo envelope modulation techniques[63] (ESEEM) confirm that there is weak coupling (1 MHz) to the axial ligand. The conserved g values in the EPR spectra indicate that the geometry of the five-coordinate species retains its near-axial symmetry.

The EXAFS analysis for Ni^{I}(OEiBC)$^-$ with pyridine shows an average equatorial metal−nitrogen bond length of 2.04 Å and one additional axial nitrogen at ~2.2 Å. The distances found in both two-shell fits indicate that the distortion in the equatorial distances could be retained in five-coordinate complexes. The quality of the data does not permit a three-shell analysis of the EXAFS data. The axial and rhombic signals observed for Ni^{I}(F430) may thus both result from five-coordinate geometries with different axial bond lengths.

The near-edge X-ray absorption measurements clearly demonstrate that Cu^{II}(OEiBC) binds a single pyridine at low temperatures, similar to the isoelectronic Ni^{I}. Optical studies of copper porphyrins in the presence of piperidine have indeed shown that Cu^{II} does not bind more than one axial ligand.[64] This behavior may be a result of the Jahn−Teller distortion preventing symmetric octahedral environments. This may have implications for the coordination and reactivity of Ni^{I}(F430) in methyl reductase.

No evidence is found for a significant splitting of the first-shell distances in Cu^{II}(OEiBC); a single average distance of 2.0 Å is found. This result agrees with the distances found crystallographically for Cu^{II}(dioxoOEiBC); bond lengths of 2.0 and 2.04 Å.[65] EXAFS measurements cannot resolve such small bond length differences (±0.02 Å from the average) and will find a single shell with a slightly enhanced disorder factor. The significant distortion observed with Ni^{I} is thus not simply an electronic effect resulting from an unpaired electron in a $d_{x^2-y^2}$

(52) Schiemke, A. K.; Shelnutt, J. A.; Scott, R. A. *J. Biol. Chem.* **1989**, *264*, 11236.
(53) Jaun, B. *Met. Ions Biol. Syst.* **1993**, *29*, 287.
(54) Jaun, B. *Helv. Chim. Acta* **1990**, *73*, 2209.
(55) Eschenmoser, A. *Ann. N. Y. Acad. Sci.* **1986**, *471*, 108.
(56) Kratky, C.; Angst, C.; Johansen, J. E. *Angew. Chem., Int. Ed. Engl.* **1981**, *20*, 211.
(57) Procyk, A. D.; Bocian, D. F. *Inorg. Chem.* **1993**, *32*, 366.
(58) We have observed similar results for Ni^{I}F430: Renner, M. W.; Furenlid, L. R.; Scott, R. A. Unpublished results.
(59) Helvenston, M. C.; Castro, C. E. *J. Am. Chem. Soc.* **1992**, *114*, 8490.
(60) Chmielewsky, P. T.; Latos-Grazynski, L.; Pacholska, E. *Inorg. Chem.* **1994**, *33*, 1922.
(61) Chmielewsky, P.; Grzeszczuk, M.; Latos-Grazynski, L.; Lisowski, J. *Inorg. Chem.* **1989**, *28*, 3546.
(62) Kirste, B.; van Willigen, H. *J. Phys. Chem.* **1983**, *87*, 781.
(63) Cornelius, J. B.; McCracken, J.; Clarkson, R. B.; Belford, R. L.; Peisach, J. *J. Phys. Chem.* **1990**, *94*, 6977.
(64) Baker, E. W.; Brookhart, M. S.; Corwin, A. H. *J. Am. Chem. Soc.* **1964**, *86*, 4578.
(65) Chang, C. K.; Barkigia, K. M.; Hanson, L. K.; Fajer, J. *J. Am. Chem. Soc.* **1986**, *108*, 1352.

highest occupied molecular orbital. It must also depend on the relative sizes and charges of the metal ions. The Ni^{I} ion has a larger covalent radius than the more positively charged Cu^{II} ion. The distortion could result from a balance between the metal–nitrogen interaction energies and the conformational energy of the macrocycle. Another possible explanation is that preferential back-bonding from one of the two d π-type orbitals (d_{xz} and d_{yz}) to ligand π-system results in two distinct sets of metal–N distances. The larger radial extent and higher energy of the d orbitals of Ni^{I} should permit it to back-bond more effectively than Cu^{II}. The optical spectra of the complexes support this contention. The main visible band of Ni(OEiBC), which corresponds to the macrocycle π to π^* transition, blue shifts by 20 nm upon reduction. The shift was suggested to result from destabilization of the π^* orbital.[32] In contrast, the main visible band of Cu^{II}(OEiBC) blue shifts by less than 3 nm upon reduction to $Cu^{I}(OEiBC)^{-}$.

A comparison is possible for the first time between Cu^{II} and Cu^{I} in the same coordination environment and geometry. Cu^{II}-(OEiBC) and $Cu^{I}(OEiBC)^{-}$ with crown ether are both four-coordinate and square-planar. The Cu^{I} complex has metal–nitrogen bond lengths 0.06 Å longer than the corresponding Cu^{II} species. This is consistent with addition of an electron to the $d_{x^2-y^2}$ orbital, which is metal–ligand-antibonding with respect to the OEiBC nitrogens.

The chemical reduction of Cu^{II} with sodium amalgam without crown ether as a sequestering agent gave rise to a large second-shell peak consistent with two sodium atoms located 2.89 Å from the copper. The absorption edge spectra also indicate the presence of atoms above and below the macrocycle plane and a slightly shifted oxidation state. There is precedent for sodium ions located near reduced metals in porphyrins. The crystal structure of an Fe^{I} porphyrin anion radical reveals two sodium atoms located 3.0 Å from the iron,[66] and the cobalt(0) tetraphenylporphyrin complex has two sodium atoms 2.96 Å from the metal.[67] In both cases the sodium atoms are located over two adjacent pyrrole nitrogens. No structural changes were observed in the Cu^{I}–macrocycle core when the sodium ions are bound, which together with the edge shift suggests at least partial charge transfer away from the metal. The presence of two sodium atoms coordinated to the copper is surprising and might indicate that the sodium atoms are shared between two coppers; however, there is no indication from the optical or NMR spectra for oligomerization of the $Cu^{I}(OEiBC)^{-}$ complexes in solution.[11]

Two previously reported observations that suggested large structural differences between the Cu^{II}- and Cu^{I}(OEiBC) complexes must be reconsidered in light of our results. The large frequency shifts observed in the RR spectra of $Cu^{I}(OEiBC)^{-}$ could reflect the presence of the sodium ion(s) that are bound to the complex when sodium amalgam is used as the reducing agent. The decreased reactivity of Cu^{I} relative to $Ni^{I}(OEiBC)^{-}$ toward CH_3I and O_2 was attributed to an activation barrier for reactions that involved reoxidation of $Cu^{I}(OEiBC)^{-}$. Large structural differences were suggested as a possible cause of the barrier. However, our results establish that the structural changes in the metal–OEiBC complexes that occur upon reduction are not markedly larger for copper than for nickel. The change in metal–N distance for copper (Δ = 0.06 Å in the presence of crown ether) is similar to that for nickel (Δ = 0.05 Å average, or Δ = 0.13 and −0.03 Å for the two sets of Ni–N distances). It is not apparent whether ion pairing of the counter cations affects the reactivity of $Cu^{I}(OEiBC)^{-}$. Decreased reactivity of Cu^{I} relative to $Ni^{I}(OEiBC)^{-}$ was observed for both sodium and tetrabutylammonium counterions, and no evidence exists for pairing with the latter. An explanation for the different reactivities consistent with our experimental results is that the short pair of Ni^{I}–N distances destabilizes the metal $d_{x^2-y^2}$ orbital and enhances metal to substrate charge transfer. Cu^{I}, in contrast, shows a symmetrical expansion of the macrocycle core and is also stabilized by its closed-shell configuration.

Conclusion

These structural studies of nickel octaethylisobacteriochlorin clearly demonstrate that even though the macrocycle is less saturated than F430, it is able to undergo similar conformational changes. Comparison of the isoelectronic Ni^{I}- and Cu^{II}-(OEiBC)'s demonstrates that the distortion observed in Ni^{I} complexes is not an electronic configuration effect, such as a Jahn–Teller distortion, but is proposed to reflect a balance between metal–nitrogen interaction energies and the macrocycle's conformational energy. The pair of short Ni–N distances in Ni^{I} complexes might enhance their reactivity in the axial direction toward substrates. This also explains the decreased reactivity of the Cu^{I} relative to Ni^{I} for these complexes. The unusual RR results reported for $Cu^{I}(OEiBC)^{-}$ are explained by the binding of sodium ions upon chemical reduction.

The X-ray absorption near-edge data clearly show that at low temperatures both the Ni^{I}- and Cu^{II}(OEiBC) complexes bind one axial ligand to form five-coordinate complexes. EXAFS and EPR measurements indicate that macrocycle cores of the four- and five-coordinate species are similar. Binding of one axial pyridine to Ni^{I} does not cause the axial to rhombic EPR spectral changes that have been observed in F430. Thus, either the axial ligand present in the active form of F430 (MCR-red2) is not nitrogenous or axial ligation of F430 in the protein is accompanied by conformational changes that alter the anisotropy of the metal.

Acknowledgment. We thank J. Fajer for helpful discussions and suggesting the crown ether as a suitable sequestering agent, C. Kratky for providing X-ray coordinates for the *ttt*- and *tct*-Ni^{II}(OEiBC) structures, and R. H. Felton for helpful suggestions. The research at Brookhaven National Laboratory was supported by the U.S. Department of Energy, Chemical Sciences Division under Contract DE-AC02-76CH00016. The work at West Virginia University was supported by Grant GM 33882 from the National Institute of General Medical Sciences. EXAFS experiments were performed at Beamlines X-9B, X-10C, X-11A, and X-19A, supported by the NIH, Exxon Corp., the DOE, and the National Synchrotron Light Source, respectively. Several helpful suggestions from the reviewers are gratefully acknowledged.

JA942064D

(66) Mashiko, T.; Reed, C. A.; Haller, R. J.; Scheidt, W. R. *Inorg. Chem.* **1984**, *23*, 3192.

(67) Ciurli, S.; Gambarotta, S.; Floriani, C.; Chiesi-Villa, A.; Guastini, C. *Angew. Chem., Int. Ed. Engl.* **1986**, *25*, 553.